Admittance spectroscopy of impurity levels in Schottky barriers

D. L. Losee

Research Laboratories, Eastman Kodak Company, Rochester, New York 14650
(Received 30 September 1974; in final form 16 January 1975)

Measurements of the complex admittance of Schottky-barrier diodes as a function of temperature provide a spectroscopy of deep trapping levels. The measurement conditions are usually close to thermal equilibrium, thus assuring the validity of equilibrium occupation probabilities. An exact (i.e., to arbitrary accuracy) solution for the junction admittance is given. The problem is reduced to solution of a simple initial-value problem, the final integration being carried out by computer. It is shown that the dispersion in capacitance due to slow trapping levels can lead to serious errors in estimates of junction doping concentrations and barrier height determinations. Examples are given for p-type ZnTe where Shockley-Read-Hall (SRH) centers are dominant and for n-type CdTe and $Cd_{1-x}ZnTe$ where double-acceptor centers are dominant. For junctions formed on CdTe : Ga it is shown that one of the steps in capacitance observed in a thermally stimulated capacitance survey is actually a high-frequency response step and is not due to slow emission from a trapping center.

PACS numbers: 85.30.H, 73.30.

I. INTRODUCTION

Deep impurity levels in semiconductors play an important role in determining virtually all semiconductor-device characteristics. In the compound semiconductors, in particular, it is important to be able to assess the number, energy, and polarity of carrier traps that may be present. These levels are likely to be present in large numbers owing to increased reactivity of component elements and the increased tendency toward formation of native defects. In this work we present a new method of surveying a material for the presence of trapping levels, which extends and supplements the methods that have previously been directed to this problem. The advantages of what we call the admittance spectroscopy method[1] are as follows: (1) Relatively shallow and/or fast levels are easily seen. (2) Quasi-equilibrium conditions are maintained, thus allowing use of thermal equilibrium statistics for the band potential calculations. (3) The measurements supplement such methods as thermally stimulated capacitance (TSCap)[2,3] and the deep-level transient spectroscopy (DLTS)[4] methods. (4) A certain amount of diode leakage conductance is tolerable. (5) The technique is spectroscopic, i.e., there is a peak observed for each energy level, the peak height is related to the number of centers (weighted according to level depth) and the linewidths may be compared with discrete level models.

A. Prior work

It has been realized for some time[5] that the band bending associated with Schottky-barrier formation offers a means of access to deep impurity levels in semiconductors without having to tamper with crystal chemistry, for example, by addition of compensating impurities or diffusion to form a p-n junction. A number of methods have been developed for study of deep levels by transient capacitance measurements.[4,6] In these studies a p-n or Schottky-barrier diode is cooled under some preset bias condition. Then the capacitance of the junction is measured as a function of time after application of a stepwise voltage change. In this way emission rates for slow centers can be followed as a function of temperature and activation energies determined. For Shockley-Read-Hall[7] (SRH) centers this amounts to a determination of the energy level of the center. A variation of this method is the TSCap[2,3] technique, where capacitance is recorded vs temperature during heating of the sample. This method, however, usually requires some assumption to be made on attempt-to-escape frequencies. Further, a corroberative thermally stimulated current (TSC) measurement is required, thus placing rather stringent requirements on tolerable diode leakage currents.

The only true spectroscopic scheme for observation of deep levels that has been proposed previously is that of Roberts and Crowell.[8] These authors noted that a change in C should occur when a junction is forward biased such that the quasi-Fermi level no longer intercepts the energy of a deep-lying level (see Fig. 1). Two assumptions must be valid for this technique to be applied: first, the deep level must be able to respond at the frequency of the ac measurement signal and second, thermal equilibrium must be maintained even though the junction is forward biased. These conditions are frequently difficult to attain. One further consideration is that the large conductance at forward bias can make the experimental measurements extremely difficult.

A hybrid of these two basic methods has been discussed by Sah and Walker,[9] the so-called "edge effect TSCap". Here a capacitance shift is observed that is associated with the movement of the Fermi energy with temperature above or below a relatively shallow level. This method, however, has little advantage over ordinary Hall-coefficient and transport-coefficient analysis. A further variation on the TSCap approach is the DLTS method developed by Lang.[4] This method has several advantages and is spectroscopic, but to be used to full advantage an abrupt p-n junction is required. It is less useful for traps with repulsive barriers to recombination since the energy-level determination is only by analysis of emission rates as a function of temperature.

Zohta[10] has suggested a method of analysis of C^{-2}-vs-V data taken first with slow voltage changes and then by means of the Copeland[11] (second harmonic) method to obtain energy depths and profiles. However, considerable analysis is required and if many levels are present

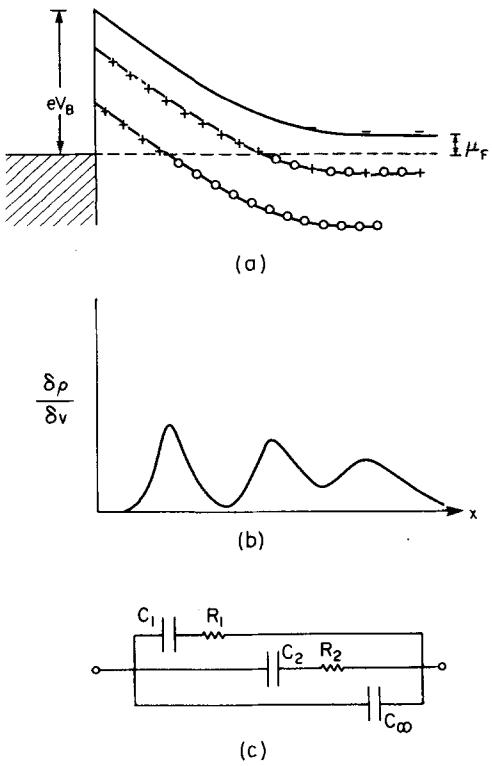

FIG. 1. Schottky-barrier diode containing deep trapping levels: (a) band potential vs distance. Barrier height V_B and Fermi energy μ_F are indicated. The shallow levels are partially ionized in the semiconductor bulk. The free-electron distribution is also indicated. (b) ac component to the charge density as a function of distance from the metal-semiconductor interface. The first two peaks are due to the discrete trapping levels and the third peak is due to the free-electron response. (c) Approximate equivalent circuit for junction admittance. The resistor values corresponding to each trapping level are such that $R_i C_i = \langle \tau_i \rangle$. The magnitude of C_i depends on the depth and concentration of the ith level. C_∞ represents the free-electron contribution. The circuit is considered approximate because there is a *distribution* of time constants contributing to the response of each level [see Eq. (18)ff].

no accurate analysis procedure is available.

B. Scope of present work

This paper presents an alternative approach that has been useful in studies of several materials. In some respects it may be viewed as a supplement to the methods outlined above, which extends the range of accessibility to analysis for defect centers in semiconductors. It will be shown that measurements of the capacitance (C) and conductive (G) components of the junction admittance at two (or more) frequencies as a function of temperature provide a spectroscopy of defect levels (principally majority-carrier traps) yielding energies, types, concentrations, and majority-carrier capture coefficients. The only additional characterization of the junction required is a measurement of the Schottky-barrier height by, for example, the internal photoemission method[12] and measurements of $C(V)$ at low frequency.

We present an exact (i. e., to arbitrary accuracy) method of solution of the transport-boundary-value problem in the small-signal approximation. For nondegenerate statistics the solution is analytic up to a single integration of a first-order *initial-value* problem, the final integration being carried out easily on a digital computer using standard subroutines. For degenerate statistics the initial-value problem contains several Fermi integrals. This exact calculation of C and G is used in the final quantitative evaluation of imperfection densities and determination of level polarity. It further permits assessment of linewidths or the degree of distribution of response times for a given level. This approach differs from previous treatments[13–16] in that trap-occupation probabilities, the free-carrier distribution, and the proper rate equations are all accurately included.

Experimental measurements are presented on two different types of centers, Shockley-Read-Hall centers in p-type ZnTe [1,17] and the slow persistent photoconductivity (double-acceptor) centers in n-type CdTe and $Cd_{1-x}Zn_xTe$ alloys.[18–20] In the latter case a comparison may be made with TSCap data. It is shown that one of the steps observed in a TSCap survey is actually a high-frequency response step, not the onset of slow emptying of a trap, but that the two possibilities may be distinguished by examination of the G component of the admittance. Finally, we present data on the frequency dispersion of capacitance in $Cd_{1-x}Zn_xTe$ junctions. The effect of this dispersion on estimates of barrier heights and net charge density in the depletion region is discussed and comparison calculations are presented.

II. THEORY

When a small ac voltage is applied to a Schottky-barrier diode, the various defect energy levels sweep through the quasi-Fermi level, thus producing an oscillation in the charge density distribution. This is illustrated in Fig. 1(b), which depicts the magnitude of the oscillation in charge density, $\delta\rho$, as a function of distance from the metal electrode. For a planar junction it is easily shown[21] that the capacitance of the diode is given quite generally by $\epsilon A/x_{cg}$, where ϵ is the low-frequency dielectric constant, A is the area, and x_{cg} is the geometrical center of gravity of the $\delta\rho$ distribution. $\delta\rho$ is peaked roughly at each point where the Fermi level passes through a trapping level, provided that level is responding at the test frequency. If the frequency of δv (the applied ac signal) or the temperature of the junction changes so that one of the levels cannot respond, then there will be a corresponding shift in x_{cg} and hence a change in C. At intermediate temperatures the change, $\delta\rho_k$, for, say, the kth level, is finite but lags δv, thus producing a real component, or loss, in the admittance. Roughly speaking, a peak in conductance should occur where $\omega\langle\tau_k\rangle = 1$. Here ω is the angular frequency and $\langle\tau_k\rangle$ is an average time constant for the kth level. (The meaning of this average will be discussed later.) Thus, if G is recorded as a function of temperature, T, at fixed frequency, a peak in G will be observed each time an $\omega\tau = 1$ condition is met.

A. Mathematical development

We wish to calculate the diode current for sinusoidal

applied voltage. The total current at all points in the physical circuit must be the same; in particular, consider the region at $x = 0^+$ (see Fig. 1), where the total current essentially equals the displacement current. We may assume that the relaxation time of the *free*-electron distribution is very short compared with the measurement frequency, i. e., the free carriers are in thermal equilibrium. Then the effects of the continuity equation are separated from the solution of Poisson's equation.[14] Since it is only the ac component of current that is of interest, we only require calculation of the ac field at $x = 0^+$.

Let ψ and φ be the dc and ac band potentials, respectively, at any point x in the junction (ψ is measured with respect to the Fermi level). ρ and $\delta\rho$ are the dc and ac charge densities, respectively. Poisson's equation may then be separted into ac and dc parts;

$$\frac{d^2\psi}{dx^2} = \frac{\rho}{\epsilon}, \quad \frac{d^2\varphi}{dx^2} = \frac{\delta\rho}{\epsilon}. \tag{1}$$

The dc solution has been presented by Roberts and Crowell[8] for the case where $\rho = \rho(\psi)$ (uniform doping), which we are considering here. For completeness we shall outline their method of solution and thus define, and show the origin of, the functions required for the ac solution.

Using the identity

$$\frac{d^2\psi}{dx^2} = \frac{1}{2}\left(\frac{d\psi}{dx}\right)^{-1}\left(\frac{d}{dx}\right)\left(\frac{d\psi}{dx}\right)^2,$$

Eq. (1) is integrated to obtain

$$\left(\frac{d\psi}{dx}\right)^2 = \frac{2}{\epsilon}\int_{\mu_F}^{\psi} (\psi')\, d\psi' \equiv H(\psi). \tag{2}$$

Note that we have implicitly made a change of variables to consider ψ as the independent variable. The integration, therefore, extends from $\psi = \mu_F$ (i. e., $x = \infty$), where $d\psi/dx = 0$, to a point in the junction where the band potential is ψ. The point $x = 0$ corresponds to $\psi = (V_B - V)$, where V_B is the metal-semiconductor barrier height and V is the dc applied bias voltage. The dc surface charge, σ, induced on the metal is $-\epsilon(d\psi/dx\,|_{V_B - V}$ and the dc capacitance is defined by

$$C_0 \equiv \frac{d\sigma}{dV} = \rho(V_s)H^{-1/2}(V_s), \tag{3}$$

where $V_s = V_B - V$. Given the energy distribution of defect levels it is thus straightforward to integrate ρ and calculate C_0. The bulk Fermi energy μ_F must, of course, be calculated beforehand to assure bulk charge neutrality. Roberts and Crowell[8] have given analytic expressions for C_0 for the case of nondegenerate statistics.

We turn now to the ac portion of Eq. (1). Here, we wish to again change variables and use ψ as the independent variable. Then

$$\frac{d\varphi}{dx} = \frac{d\varphi}{d\psi}\frac{d\psi}{dx} \tag{4a}$$

and

$$\frac{d^2\varphi}{dx^2} = \frac{d\varphi}{d\psi}\frac{d^2\psi}{dx^2} + \frac{d^2\varphi}{d\psi^2}\left(\frac{d\psi}{dx}\right)^2. \tag{4b}$$

Substituting from Eqs. (1) and (2),

$$\frac{d^2\varphi}{dx^2} = \frac{\rho(\psi)}{\epsilon}\left(\frac{d\varphi}{d\psi}\right) + H(\psi)\frac{d^2\varphi}{d\psi^2} = \frac{\delta\rho}{\epsilon}. \tag{5}$$

We now make a small-signal approximation and expand $\delta\rho$ in a Taylor series, retaining only the linear term,

$$\delta\rho = \varphi F(\psi, \omega). \tag{6}$$

$F(\psi, \omega)$ is the first-order coefficient of φ in the expansion of $\delta\rho$. In the low-frequency limit, $F(\psi, \omega)$ will be equal to $d\rho/d\psi$. Expressions for $F(\psi, \omega)$ will be given later [Eq. (18) ff and Appendix A].

Since we wish to calculate the diode admittance we only need the ratio of alternating current to applied alternating voltage. We note that the current density $j = i\omega\sigma_{ac}$ and $\sigma_{ac} = -\epsilon(d\varphi/dx)\,|_{x=0}$. Thus the admittance per unit area is given by

$$Y = -i\omega\epsilon\left(\frac{1}{\varphi}\frac{d\varphi}{dx}\right)\Bigg|_{x=0} = -i\omega\epsilon\frac{d\psi}{dx}\left(\frac{1}{\varphi}\frac{d\varphi}{d\psi}\right)\Bigg|_{x=0}. \tag{7}$$

It is convenient to make one further change of variables, defining,

$$W(\psi) = \left(\frac{1}{\varphi}\frac{d\varphi}{d\psi}\right)^{-1}. \tag{8}$$

Then

$$Y = -i\omega\epsilon\{[H(\psi)]^{1/2}/W(\psi)\}\,|_{V_B - V} \tag{9}$$

and from Eqs. (5) and (6), W satisfies the equation

$$\frac{dW}{d\psi} = 1 + \frac{\rho}{\epsilon H}W - \frac{F}{H}W^2. \tag{10}$$

This is a first-order initial-value problem, which is solved by integrating from $\psi = \mu_F$ to $\psi = V_B - V$. It must be remembered, however, that the functions F and W are complex. This means that Eq. (10) is actually a coupled pair of first-order equations. This poses no complication, however, since standard numerical routines are available for solution of such systems of equations. Expressions for ρ, H, and F are given in Appendix A.

To ascertain the proper initial value to be used in integrating Eq. (10) we consider the boundary conditions in the junction for $\psi = \mu_F$ (i. e., as $x \to \infty$). Consider the functions H and F. Since μ_F is defined by the condition of charge neutrality, then to first order ρ is linear in $\psi - \mu_F$ and $H \doteq \rho'(\psi - \mu_F)^2/\epsilon$. Then the requirement that W and W' be well defined requires $W \propto \psi - \mu_F$ near $\psi = \mu_F$. Thus, the initial condition for Eq. (10) is $W = 0$ at $\psi = \mu_F$. On expanding W, H, and ρ about the point $\psi = \mu_F$, we find the flat-band admittance

$$Y_{fb} = i\omega\epsilon[F(\mu_F, \omega)]^{1/2}, \tag{11}$$

which is easily shown to yield the standard expression for flat-band capacitance, $C_{fb} = \epsilon^{1/2}[(d\rho/d\psi)\,|_{\mu_F}]^{1/2}$, in the low-frequency limit.

B. Specific models

1. Energy-independent capture

Consider a set of SRH centers with hole- and electron-capture cross sections that are effectively energy in-

dependent. Then the electron occupation n_t of the N_t traps is governed by

$$\frac{\partial n_t}{\partial t} = nC_n(N_t - n_t) - e_n n_t - C_p p n_t + e_p(N_t - n_t). \tag{12}$$

Here C_n, e_n, C_p, and e_p are the capture coefficient and the emission rate for electrons and holes, respectively, and n and p are the free-electron and -hole densities. In the small-signal approximation n_t, n, and p are close to their thermal equilibrium values, n_0 and p_0, and this equation may be linearized in the perturbations, δn_t, Δn, and Δp. Since occupation probabilities depend on the band potential, the small-signal condition is that $\varphi \ll kT$ where φ is the ac potential at the point where μ_F intersects the trap energy level. For the free carriers we are assuming thermal equilibrium; thus, for nondegenerate statistics

$$\Delta n = -n_0\,\varphi/kT \quad \text{and} \quad \Delta p = p_0\,\varphi/kT. \tag{13}$$

Then substituting in Eq. (12) and solving we find

$$\delta n_t = -N_t(\varphi/kT)\,\tau[f_t C_n n_0 + (1-f_t)\,C_p p_0]/(1+i\omega\tau), \tag{14}$$

where

$$\tau^{-1} = C_n n_0 + C_p p_0 + e_n + e_p \tag{15}$$

and

$$f_t = [1 + \beta \exp(E_t - \psi)/kT]^{-1}. \tag{16}$$

Here f_t is the ionization probability for donorlike traps and the probability of neutrality for acceptorlike traps. β is the degeneracy factor.

Several comments are now in order: (i) If the dominant process governing the trap occupation is hole capture and emission (taking the material as n type for discussion purposes), then the magnitude and frequency dependence of δn_t will be light sensitive, first through photoionization and second through increased hole capture when band-gap illumination is used. (ii) In the dark, the emission and capture coefficients are related (for nondegenerate statistics) by

$$e_n/C_n = N_c \exp(-E_t/kT) \tag{17a}$$

and

$$e_p/C_p = N_v \exp[-(E_g - E_t)/kT]. \tag{17b}$$

Here E_g is the energy gap, and N_c and N_v are the conduction-band and valence-band densities of states, respectively. We now note that the level N_t will contribute to C and G only if the band bending is sufficient to allow the Fermi level to cross the trapping level.[8] This means that minority-carrier emission is a possibility only if the observed activation energy for τ is greater than $E_g - V_B$. In most cases this is sufficient to distinguish minority-carrier processes. (iii) The charge state of the centers may frequently be deduced from the magnitude of the capture coefficient. It will be seen that this coefficient is deduced from the intercept on the $1/T$ axis of a plot of the position of the loss peak in $G(T)$.

We consider now the case where only majority-carrier trapping contributes, the semiconductor is nondegenerate, and there is no illumination. Then using Eq. (17a), Eq. (14) reduces to

$$\delta n_t = -N_t \frac{\varphi}{kT} \frac{f_t(1-f_t)}{1 + i\omega[(1-f_t)/C_n n_0]} = -N_t \frac{\varphi}{kT} \frac{f_t(1-f_t)}{1 + i\omega(f_t/e_n)}. \tag{18}$$

For several discrete trapping levels we have a sum of terms similar to Eq. (18); these added to the free-electron change Δn then give $F(\psi, \omega) = -q(\Delta n + \sum_i \delta n_{ti})/\epsilon$, where δn_{ti} is the perturbation in occupation of the ith level.

Note that δn_t is a peaked function, reaching a maximum approximately where $f_t = \frac{1}{2}$. Thus, the average value of τ is given by

$$\langle \tau \rangle^{-1} \approx 2C_n N_c \exp(-E_t/kT)\,\beta^{-1}. \tag{19}$$

Each peak in conductance at temperature T_p may thus be plotted as $\omega T_p^{-3/2}$ vs $1/T_p$ to yield a straight line with slope $-E_t$ and intercept determining C_n. The factor $T_p^{-3/2}$ takes into account the temperature variation of N_c. Immediately we may see the range of usefulness of the present method of deep-level spectroscopy by taking $N_c \sim 10^{17}$, $6\times10^2 \leq \omega \leq 6\times10^5$, and $T < 400\,^\circ$K. For Coulombic centers (attractive) the capture coefficient[22] is $\sim 5\times10^{-6}$ cm^3/sec giving a maximum depth for a trap to be seen as ~ 0.7 eV; for a neutral center the capture coefficient is greatly reduced, say 5×10^{-12}, this puts an upper limit of ~ 0.25 eV for the level depth. Slower levels, however, are studied more easily by the transient capacitance techniques described elsewhere.[2-4] The main strength in the present scheme is that Coulombic (fast capture) levels are now more accessible.

2. Energy-dependent capture

We consider now the case of strongly energy-dependent capture probability such as is encountered with the "double-acceptor" centers in n-type materials.[18,20] These centers are characterized by an energy level close to the conduction band edge but with a repulsive potential to recombination. The release rate is temperature dependent with an activation energy, E_a, in the range 0.3—0.5 eV[19,20] (for CdTe, for example). The capture cross section as a function of energy is roughly a step function at energy $E = E_c + E_B$, where E_c is the band-edge energy and E_B is the effective barrier around the center. It is then easy to show that the right-hand expression in Eq. (18) applies, giving

$$\delta n_t = N_t \frac{\varphi}{kT} \frac{f_t(1-f_t)}{1 + i\omega f_t\,\tau_0 \exp(E_a/kT)}, \tag{20}$$

where τ_0 is a constant characteristic of the emission rate. In this case note that the activation energy for τ bears no obvious relation to the actual position of the energy level as contained in the f_t factors.

C. General features of C and G vs T

There are three factors that determine the magnitude of the change in C, ΔC_i, on passing through the $\omega\tau_i = 1$ condition for the ith level: the number of states, the location, x_t, of the point where $\psi(x_t) = E_t$, and the magnitude of $\varphi(x_t)$. φ goes to zero in the semiconductor bulk and x_t goes to zero near $E_T = V_B$. ΔC is calculated

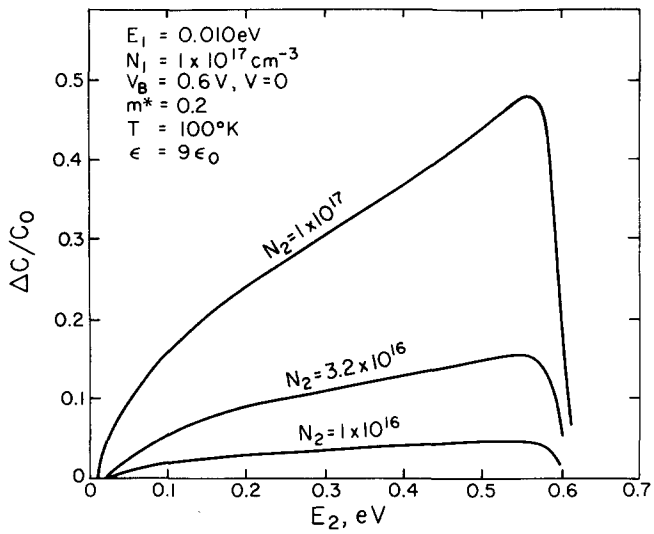

FIG. 2. Relative change $\Delta C/C_0$, expected in capacitance due to freeze out of deep-level response. Curves are plotted as a function of level depth for three concentration ratios. The shallow level at 0.010 eV is taken to be fully responsive at the test frequency. Relevent parameters for the calculation are indicated.

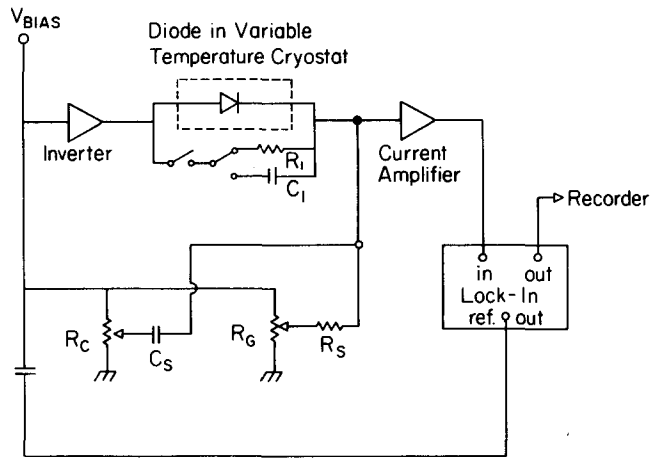

FIG. 3. Schematic diagramof apparatus used to record admittance components. The sample diode is held in a variable temperature Dewar; capacitative and conductive components are recorded as the temperature is scanned. The phase of the lock-in amplifier is adjusted for zero change when either R_1 (for capacitance measurements) or C_1 (for conductance measurement) are added in parallel to the diode under test. The ac signal is taken from the reference output of the lock in. The inverter amplifier changes the phase of the ac signal by 180° so that the potentiometer network (R_c, C_s, R_G, and R_s) may be used to provide zero offset or null for calibration purposes.

for a few typical cases in Fig. 2 as a function of level depth and concentration. The sensitivity of the method is relatively constant in E_t and nearly linear in impurity concentration for the case where the density of traps is less than the depth of the shallowest donor (or acceptor) level.

The magnitude of the peak height in G is easily estimated considering the approximate equivalent circuit in Fig. 1(c). For the ith level the value of τ_i is being varied as a function of T. The real component in the admittance reaches a peak value of $\frac{1}{2}\omega\Delta C_i$, the width at half-maximum being given roughly by the conditions $\tau_i = (2 \pm \sqrt{3})\omega^{-1}$. Evidently the peak width, ΔT, on a plot of G vs T will depend on the energy dependence of τ; a rough estimate is $\Delta T \approx (2.6E/k)[\ln(\omega\tau_0)]^{-2}$, where τ_0 is the prefactor in the expression $\tau = \tau_0 \exp(E/kT)$.

Finally, for nondegenerate materials, there will be a low-temperature peak in G when the spreading resistance of the diode, $r/2d$, equals $1/\omega C$. Here d is the diameter of a circular contact and r is the resistivity of the semiconductor. At very low temperatures the measured capacitance drops to nearly zero, limited effectively by the geometry and spacing of the Schottky contact with respect to the Ohmic return contact.

III. EXPERIMENTAL DETAILS

A. Instrumentation

In order to apply the theory developed in Sec. II to the quantitative analysis of material properties the small-signal condition of $\varphi \ll kT$ must be satisfied. This condition is guaranteed if the applied ac signal $v \ll kT/e$. For the present work the circuit diagrammed in Fig. 3 was used to apply ac and dc bias to the diode under test. The resulting currents are amplified and the phase is sensitively detected by a lock-in amplifier. The phase is adjusted by switching either a resistor or a capacitor in parallel with the sample and adjusting for no change in output. In this way loss factors up to ~30 can be accommodated. Calibration and compensation for stray circuit elements are accomplished by adjustment of potentiometers R_c and R_G, which proportion v across C_s and R_s, a standard capacitor and resistor, respectively.

The diodes are maintained in a variable-temperature cryostat in a "three-terminal capacitor" geometry. Temperatures are monitored by a calibrated Cu-constantan thermocouple fastened to the sample by G. E. 7031 varnish.

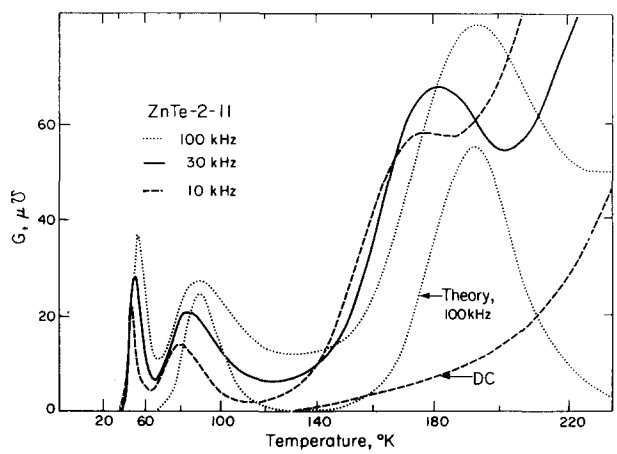

FIG. 4. Conductance vs temperature at $V = 0$ for a Schottky-barrier Au-ZnTe junction. Ordinate scale is for 100-kHz measurements; 30- and 10-kHz scales are reduced by 2.8 and 5.8, respectively. The dc conductance of the diode is estimated as shown. The conductance calculated according to the theory developed in Sec. II, using the parameters discussed in the text, is shown for comparison.

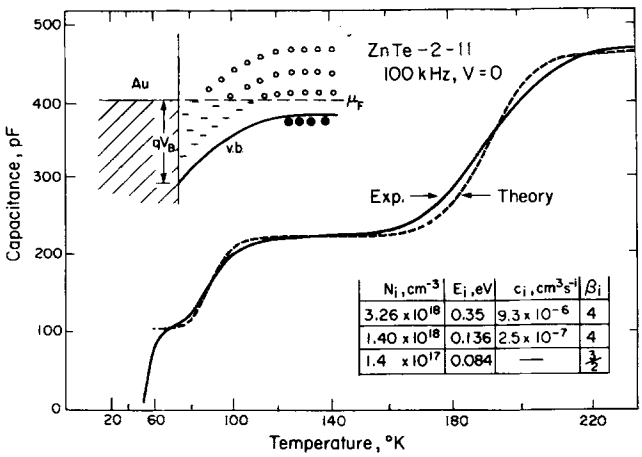

FIG. 5. Capacitance vs temperature (at $V=0$) for the diode of Fig. 4. The parameters used in the calculation to generate the theoretical curve are indicated in the inserted table. The energy levels, concentration, and barrier heights are determined as discussed in the text. The band diagram for this p-type material is shown in the upper left. Junction area is 3.2×10^{-4} cm^2.

B. Diode fabrication

Sample materials used in this work were as-grown ZnTe crystals,[17] grown from Te solution, nominally undoped and p type, and Bridgman-grown n-type CdTe and $Cd_{1-x}Zn_xTe$ alloys, doped in the melt with Cl or Ga and annealed in saturated Cd vapor at 800 °C.[23] Bars of these materials were cut and pairs of Ohmic contacts applied. The bars were then either cleaved in air or under vacuum and Au contacts were deposited in an ion-pumped evaporator system. Contact to the metal electrode was made by means of a spring-tensioned gold wire probe.

IV. ZnTe RESULTS

A. Preliminary analysis

Conductance vs temperature at zero bias for a Au-ZnTe junction is displayed in Fig. 4. For this sample, three prominant conductance peaks are observed, the peak positions and peak heights being frequency dependent. Steps in the capacitive component of the admittance are observed corresponding to the conductance peaks and are shown in Fig. 5 for a measurement frequency of 100 kHz.

The low-temperature photoconductive behavior of ZnTe [17] shows none of the behavior characteristics of trapping centers with repulsive potentials to recombination. Thus, it is reasonable to begin analysis of $G(T)$ assuming SRH centers. Further, the material exhibits p-type conductivity and the junction admittance is insensitive to band-gap illumination. Thus, the centers involved are hole traps and we must adapt Eq. (19) accordingly. Then a plot of $\omega/T_p^{3/2}$ vs $1/T_p$ yields a straight line with slope corresponding to the trap depth (with respect to the valence band) and an intercept at $1/T_p = 0$ which is equal to $9.7 \times 10^{15} m^{*3/2} C_{pi} \beta_i$ for the ith level. Such a plot is shown in Fig. 6 for the data of Fig. 1. The capture coefficients deduced from this analysis are 9.3×10^{-6} and 2.5×10^{-7} cm^3/sec for the levels at 0.34 and 0.136 eV, respectively. These capture coefficients are comparable in magnitude to those observed in other semiconductor materials for charged-Coulombic-attractive centers,[22] thus indicating that the levels are acceptor levels (levels that are neutral when occupied by a hole). The degeneracy factors for these levels have been taken equal to 4, as is expected for acceptor levels.[24] The observed energy levels and their relative concentrations are in reasonable agreement with the photoconductivity results of Fischer *et al.*[17] made on similar material. They found the dominant hole traps at 0.25 and 0.13 eV.

The low-temperature peak in Fig. 1 is due to the spreading resistance of the bulk material, the activation energy for this peak corresponding roughly to the activation for bulk conductivity. In the absence of direct mobility data this can be used to estimate roughly the energy of the shallow acceptor level. In this case we find 0.084 eV, which is in reasonable agreement with the more detailed analysis carried out by Fischer *et al.*[17] and Larsen, Varotto, and Stevenson,[25] who found the shallow acceptor at 0.060 eV. This level is believed to be the second ionization level of a Zn-vacancy double acceptor; hence a degeneracy factor of $\frac{3}{2}$ is expected.[24]

B. Numerical comparisons

Roberts and Crowell[8] have shown that at higher temperatures, when all defect levels are responding at the test signal frequency, the plot of C^{-2} vs V remains linear but the voltage axis intercept, V_0, is no longer given by $V_B - \mu_F - kT$, but is, in fact, reduced to lower values. Their expression (30) gives, for a set of donor levels,

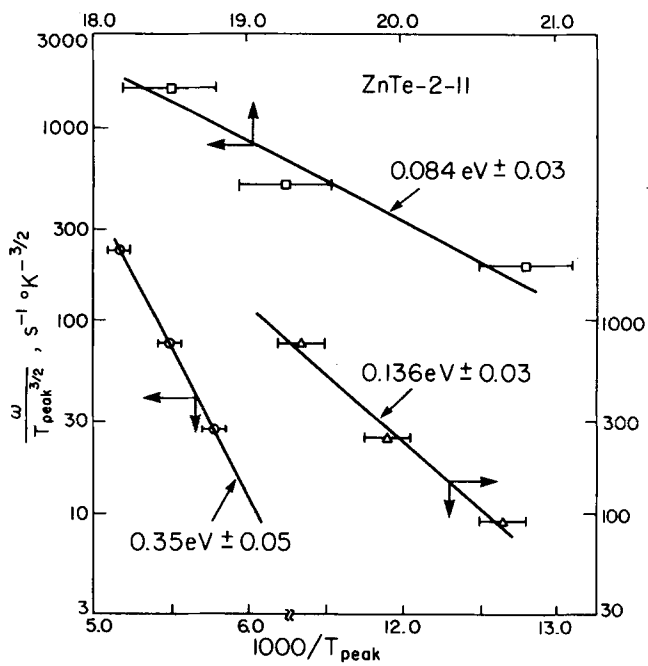

FIG. 6. Plot of $\omega_p^{-3/2}$ vs reciprocal peak temperature, T_p^{-1}, to determine level depths and capture coefficients for the data shown in Fig. 4.

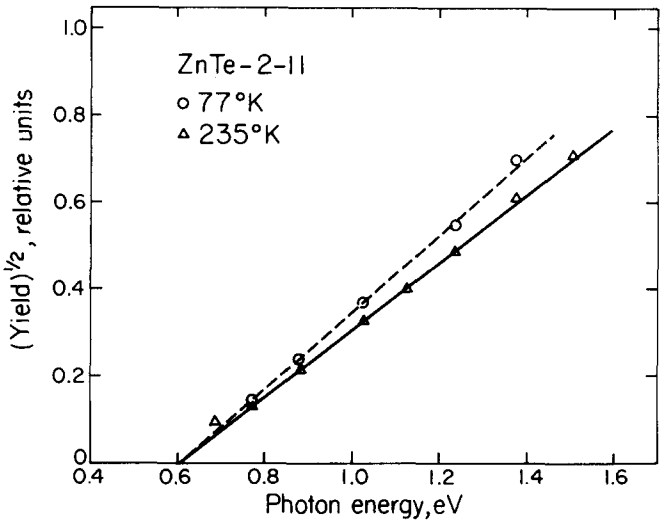

FIG. 7. Photoresponse for junction of Figs. 4 and 5. Intercept determines the metal-semiconductor barrier height, 0.60 eV in this case.

$$V_0 = V_B - \mu_F + \frac{kT}{q}\left(\sum_i \{N_i[\ln f_i(\mu_F) - f_i(\mu_F)]\}\right)\left(\sum_i N_i\right)^{-1}, \qquad (21)$$

where f_i is the ionization probability for a donorlike level. N_i is the concentration of the ith level. If the deep levels (where $f_i \ll 1$) are dominant, clearly there will be a reduction in V_0 and the C^{-2}-vs-V plot no longer serves to determine the barrier height. In this case a Fowler plot[12] of photoelectronic yield is required to determine the true barrier potential V_B. A Fowler plot analysis is shown for the present junction in Fig. 7. The value $V_B = 0.60$ eV is in reasonable agreement with the measurements of Baker and Milnes[26] (0.64 eV) and Mannex[27] (0.62 eV) for chemically prepared surfaces.

To complete the analysis it is necessary to make numerical comparison to the measured $C(T)$ shown in Fig. 5 using the theoretical model developed in Sec. II. As a boundary condition for the fitting we note that the slope of dC^{-2}/dV in the low-frequency limit still determines the net charge density at the surface. We then find from Fig. 8 that $N_i = 4.8\times10^{18}$ cm^{-3}. Using this value for $\sum N_i$ and the energy levels determined in the preliminary analysis, the values of N_i are varied to obtain a good fit of the computed $C(T)$ to the experimental results. The fitted curve and the acceptor concentrations so determined are shown in Fig. 5. To establish the consistency of the calculated densities and energy levels we may compare the room-temperature (low-frequency) $C(V)$ data with the calculated values. In this case we find $V_0 = 0.28$ V, as calculated from Eq. (21), in excellent agreement with experiment.

As a final comparison to theory the computed loss at 100 kHz is shown in Fig. 4. The calculational details are presented in Appendix B. The magnitudes of the computed loss peaks are in excellent agreement with the experimental results. The measured linewidths are somewhat larger than predicted, indicating a total spread in recombination times of approximately a factor

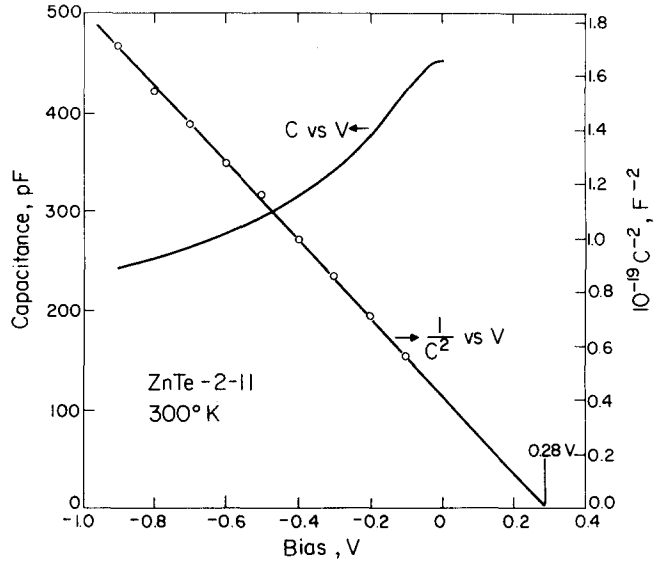

FIG. 8. Measured and calculated $C(V)$ in the low-frequency limit (100 kHz, 300°K in this case) for the Au-ZnTe junction of Figs. 4–7. The circles plot the recorded $C(V)$ as C^{-2}-vs V. The straight line was generated using the measured barrier height (0.60 eV) and level depths (see Fig. 6) and the fitted concentrations. The voltage axis intercept, 0.28 V, is shifted significantly from $V_B - kT - \mu_F$ as discussed in the text. The agreement between theory and experiment indicates the self-consistency of the level and concentration and energy determinations.

of 4. This is not surprising in view of the random distribution of centers and the corresponding fluctuations in the local free-charge density. (The Thomas-Fermi screening length is ~50 Å at room temperature for 1×10^{17} cm^{-3} free carriers).

V. CdTe AND $Cd_{1-x}Zn_xTe$ RESULTS

A. Properties of double-acceptor materials

CdTe and $Cd_{1-x}Zn_xTe$, when doped with Cl or Ga, are

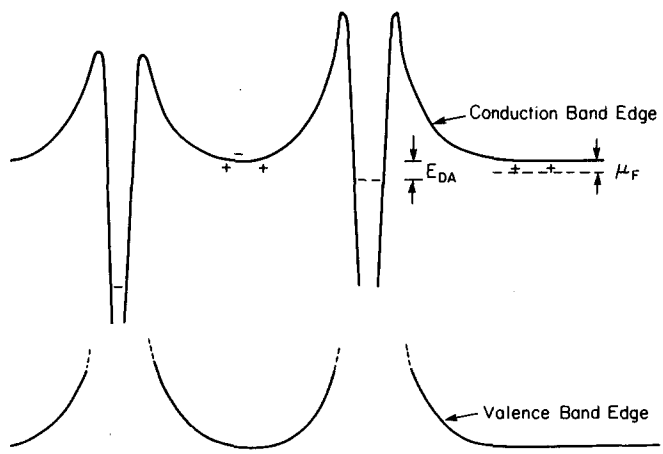

FIG. 9. Schematic band diagram of double-acceptor centers. The ground state of the doubly occupied center, indicated at the right, is close to the conduction band edge. The singly occupied center, indicated at the left, is surrounded by a repulsive barrier with respect to electrons. The shallow donors, which maintain the n-type behavior, are also indicated.

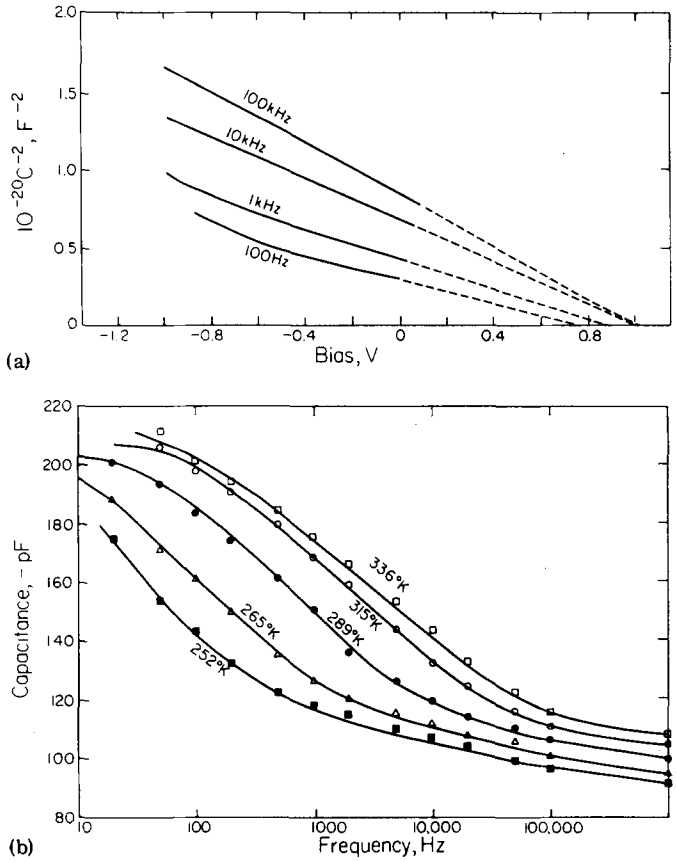

FIG. 10. (a) Capacitance at zero bias for diode on $Cd_{0.9}Zn_{0.1}Te$: Cl as a function of frequency and temperature. The diode area is 5.04×10^{-4} cm^2. (b) Frequency dependence of $1/C^2$ vs V. Note that the high-frequency plot differs significantly in both slope and intercept from the low-frequency plot. Note too that 100 Hz is still somewhat removed from being in the low-frequency limit regime. The barrier height for this diode is 0.71 eV as determined by photoresponse measurements.

n-type semiconductors but exhibit extremely long photoconductive lifetimes at reduced temperatures.[18–20] This behavior has been attributed to a dominance of the electrical properties by double-acceptor (DA) centers.[18,20] The ground state of the double acceptor is double occupied by electrons and is characterized by a small thermodynamic energy for conversion to the singly ionized state. A schematic band diagram for the double-acceptor center is given in Fig. 9. The long photoconductive decay times are a result of the low probability for hole emission to the valence band and the repulsive Coulomb barrier to electron recombination. The n-type conductivity for these materials is due to shallow donors, which are present in numbers sufficient to raise the Fermi level close to the conduction band.[28] Detailed transport studies and transient capacitance experiments have established the energy levels and emission rate activation energies as a function of dopant species and Zn content.[23,28]

B. Capacitance dispersion and barrier heights

In Schottky diodes formed on $Cd_{1-x}Zn_xTe$ a large dispersion is observed in the capacitance at temperatures in the range from − 50 to + 50 °C. Some typical results for $x=0.10$ are shown in Fig. 10. The data in Fig. 10(a) correspond to zero bias voltage. At room temperature it is seen that low frequency means frequencies well below about 100Hz. Thus, concentrations and barrier height estimates cannot be made accurately at higher frequencies. The magnitude of the dispersion and its effect on estimates of V_B and N is illustrated in Fig. 10(b). It is clear from these data that the barrier height must be determined by internal photoemission and in this case it is found to be 0.71 eV. It is seen that use of the high-frequency $1/C^2$ plot to determine N_D-N_A can lead to errors of nearly a factor of 2. Only in the low-frequency limit can this plot give the correct concentration and barrier height.

In Fig. 11 we plot the results of a model calculated[29] using the theory of Sec. II with parameters appropriate for the junctions of Fig. 10. The emission rate for the double-acceptor centers is known from previous work[23] to be given by $1.0\times10^{10}\exp(-0.45/kT)$ sec^{-1} where kT is expressed in eV and we have taken[23] the number of compensating donors to be just sufficient to fill the double acceptors at $T=0$. We see that the calculated

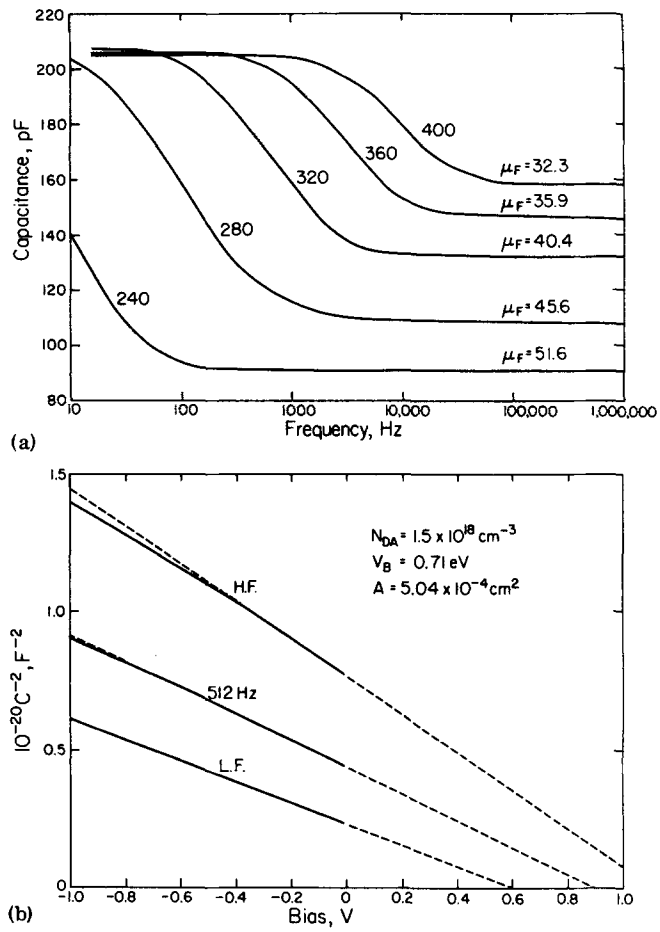

FIG. 11. (a) Calculated dispersion in capacitance using parameters appropriate to the diode of Fig. 10. ($\epsilon=9.65\epsilon$; $m^*=0.096$, $V_B=0.71$, $N_{DA}=1.5\times10^{18}$ cm^{-3}). The energy level of the double-acceptor levels has been characterized with binding energy 0.21 eV and effective degeneracy factor $\beta^*=0.16$ (Ref. 28). Fermi energies are in meV. (b) Calculated $1/C^2$ vs V for same parameters.

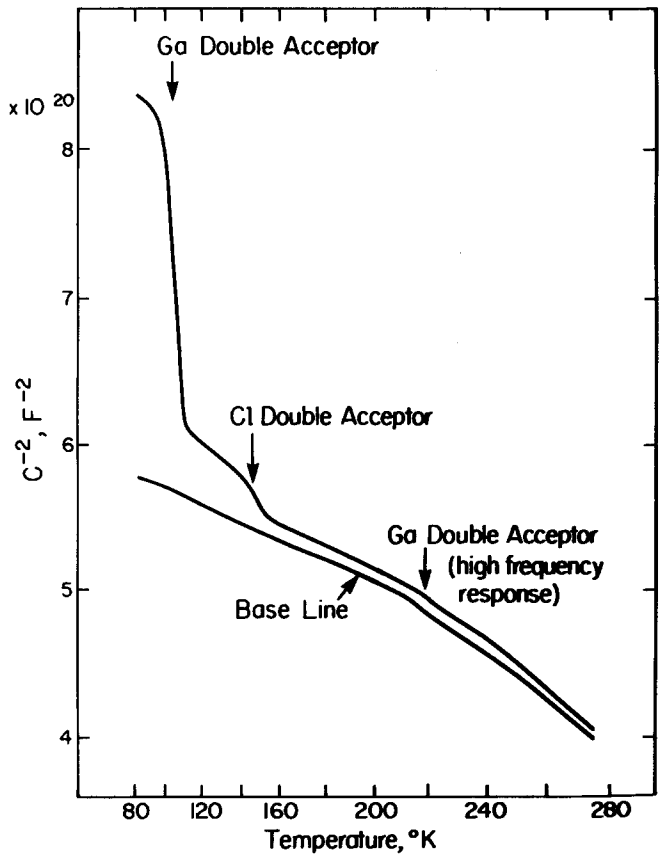

FIG. 12. TSCap data for Au on CdTe:Ga. This Ga-doped material also contains some Cl impurity (Ref. 26). The Ga- and Cl-associated double acceptors empty at 100 and 150°K, respectivley. The additional structure at 220°K is due to the response of the Ga-associated double acceptor to the test signal. The diode was cooled in the dark at zero bias, -0.6 V applied and heated. The base line results from the same cycle except that it was cooled with -0.6 V bias. The test frequency is 100 kHz, diode area 1.74×10^{-4} cm^2.

results qualitatively reproduce the behavior observed in Fig. 10, both in the order of magnitude of the dispersion in C and the spread of slopes and intercepts in the C^{-2}-vs-V plot.

The observed width of the dispersive region in C is much larger than that calculated on the basis of a single emission rate and a smooth junction potential. The width of the dispersion may be qualitatively understood by consideration of the discrete nature of the charge density associated with localized centers in the depletion region and the finite screening length associated with the free electrons. For 10^{18}-cm^{-3} centers the mean spacing between centers is approximately 31 Å. The Thomas-Fermi screening parameter varies from about 26 to 100 Å for free-carrier concentrations between 1×10^{18} and 5×10^{16} cm^{-3}, respectively. This leads to fluctuations in the local potential at any given center of about 0.040 eV. Correspondingly, fluctuations are expected in the local recombination times. The magnitude of the excess dispersion width, roughly about a factor of 20, is consistent with such potential fluctuations.

C. Comparison with TSCap data for CdTe:Ga

Sah and co-workers[6] and Buehler[3] have used the thermally stimulated capacitance method to detect deep-lying centers in silicon. In a survey of the properties of CdTe:Ga the thermally stimulated capacitance data shown in Fig. 12 were obtained. The dominant trap-emptying process occurs at about 100°K in this material owing to the Ga-associated[19] double acceptor.[28] However, a small shoulder is observed near 220°K. A casual interpretation of this shoulder would be to attribute it to a second slow center with activation energy for emptying roughly twice that of the dominant center. The confirming thermally stimulated current measurements in this case are impossible owing to the relatively high conductance of the junction (probably due to thermally assisted tunneling). Careful measurement of the conductance as a function of temperature reveals that associated with this capacitance shoulder (also seen at zero bias) is a peak in conductance. This is shown in Fig. 13. The temperature at the conductance peak is in good agreement with the time constant expected for the emission from the shallow Ga-associated double acceptor. The calculated conductance, using measured values of concentrations and emission rates, is shown in the lower half of Fig. 13. Here the precise value for the double-acceptor binding energy has been adjusted to reproduce the magnitude of the conductance peak height. The binding energy, so determined, is -0.025 eV with

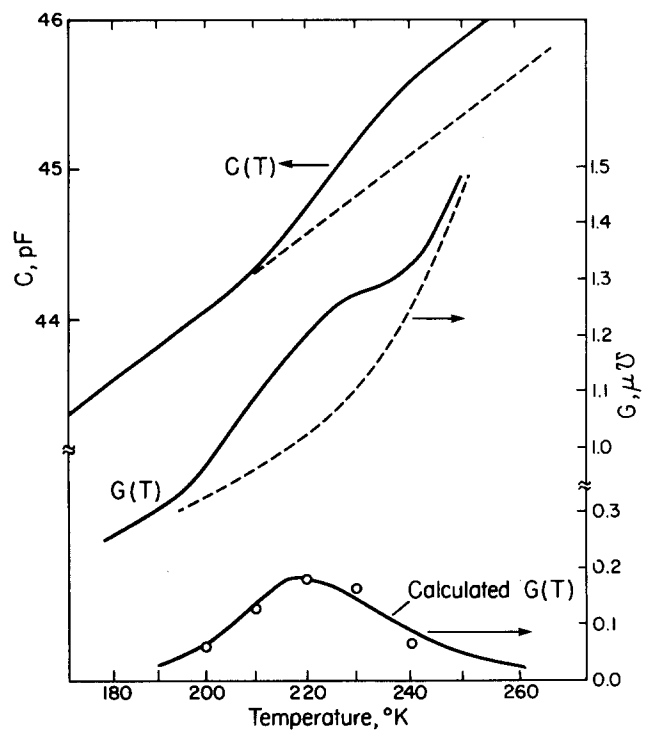

FIG. 13. Expanded view of $C(T)$ and $G(T)$ variation at 100 kHz due to the Ga-associated double acceptor. The dashed lines are estimates of the background (low-frequency) capacitance and conductance. In the lower part of the figure $G(T)$ is calculated; the points are the result of subtraction of the estimated background conductance from the measured $G(T)$. The measured concentration, 6.32×10^{17} cm^{-3}; barrier height, 0.70 eV. and emission rate $[10^{10}\exp(-0.317/kT)$ (Ref. 28)] were fixed. The energy and effective degeneracy factor used to fit the data is $E_{DA}=-0.025$ eV and $\beta^*=0.35$, in reasonable agreement with other work (Refs. 19 and 28).

an effective degeneracy factor, $\beta^* = 0.35$. [The effective degeneracy factor is $g\exp(E'/k)$, where E' is the temperature derivative of the binding energy.] Here β^* was taken to be the same as that determined by MacMillan.[19] The energy -0.025 eV places the level slightly above the Γ minimum. Iseler *et al.*[19] estimated 0.00 eV for the binding energy, which may be considered to be in reasonable agreement in view of the difficulties in determining such levels in degenerate and near-degenerate materials. The observation of the conductance peak confirms the origin of the shoulder in the TSCap data.

VI. CONCLUSIONS

Measurements of junction admittance as a function of temperature and frequency may provide a spectroscopy of slow responding levels in Schottky-barrier junctions. A method for exact calculation of junction admittance including proper statistics and rate equations is presented. It is demonstrated that slow responding levels can lead to serious errors in both concentration estimates and barrier height estimates. Experimental results and analyses have been presented for several materials, including materials with double-acceptor centers. Comparisons between calculated and observed linewidths have been made. Finally, it is shown that high-frequency response effects may add to structure in TSCap surveys.

ACKNOWLEDGMENTS

The author is grateful to D. K. Ranadive and Y. T. Tan for providing sample materials and to J. R. Fischer for assistance with preparation of Ohmic contacts. H. K. Bücher, B. C. Burkey, J. R. Fischer, R. P. Khosla, and G. L. Lubberts have contributed through many stimulating discussions.

APPENDIX A: EXPRESSIONS FOR $\rho(\psi)$, $H(\psi)$, AND $F(\psi,\omega)$

A. Nondegenerate statistics

For nondegenerate statistics expressions for $\rho(\psi)$ and $H(\psi)$ have been worked out by Roberts and Crowell.[8]

$$\rho = q\sum_{\text{donors}} N_i f_i(\psi) - q\sum_{\text{acceptors}} N_i[1-f_i(\psi)] - N_c\exp[-(\psi+\mu_F)/kT], \tag{A1}$$

where q is the electronic charge, N_i is the ith level concentration, $1-f_i$ is the probability for electron occupation, N_c is the conduction-band density of states, and μ_F is the Fermi level (in eV). Note that $\rho(\mu_F)=0$. Integrating Eq. (A1) yields

$$H(\psi) = \frac{-2q}{\epsilon}\sum_d N_i\{(\psi-\mu_F) - kT\log[f_i(\psi)/f_i(\mu_F)]\} + \frac{2q}{\epsilon}kT\sum_a N_i\log[f_i(\psi)/f_i(\mu_F)] + kTN_c\frac{2q}{\epsilon}[\exp(\mu_F/kT) - \exp(-\psi/kT)], \tag{A2}$$

where kT is expressed in volts.

For the nondegenerate case $F(\psi,\omega)$ has been given in Eq. (18) ff.

B. Degenerate statistics

For degenerate statistics the free-electron contributions to ρ, H, and F must be calculated more accurately using the Fermi integrals,[30] $\mathcal{F}_{1/2}(\psi/kT)$.

$$\rho(\psi) = -q\sum_d N_i f_i(\psi) + q\sum_a N_i[1-f_i(\psi)] + qN_c\mathcal{F}_{1/2}(\psi/kT). \tag{A3}$$

To find $H(\psi)$ this expression may be integrated once to give

$$H(\psi) = -\frac{2q}{\epsilon}\sum_d N_i\left[(\psi-\mu_F) - kT\log\left(\frac{f_i(\psi)}{f_i(\mu_F)}\right)\right] + \frac{2q}{\epsilon}\sum_a N_i\log\left(\frac{f_i(\psi)}{f_i(\mu_F)}\right) + kT\frac{2q}{\epsilon}\frac{N_c}{\Gamma(3/2)}\int_0^\infty \epsilon^{1/2}\left[\frac{\psi-\mu_F}{kT} + \log\left(\frac{1+\exp(\epsilon+\mu_F/kT)}{1+\exp(\epsilon+\psi/kT)}\right)\right]d\epsilon. \tag{A4}$$

Assuming rapid response for the free-electron contributions we differentiate the free-carrier contribution to $F(\psi,\omega)$ and finally obtain

$$F(\psi,\omega) = -\frac{q}{\epsilon kT}\sum_i \frac{N_i f_i(\psi)[1-f_i(\psi)]}{1+i\omega f_i(\psi)/e_i} - \frac{q}{\epsilon kT}\frac{N_c}{\Gamma(3/2)}\int_0^\infty \epsilon^{1/2}\frac{\exp(\epsilon+\psi/kT)}{1+\exp(\epsilon+\psi/kT)}d\epsilon. \tag{A5}$$

APPENDIX B

In this Appendix the calculational details for the theoretical comparisons shown in Figs. 4 and 5 are outlined.

The input parameters to the admittance calculation are the level densities N_1, N_2, and N_3; their energies and respective capture coefficients are provided by the preliminary analysis discussed in Sec. IV. The calculation further requires the valence-band density-of-states effective mass (0.728 for ZnTe[31]) and specification of the temperature.

The first step is to compute the Fermi energy from the bulk charge neutrality condition,[30] $\rho(\mu_F)=0$. Modification of the expressions of Appendix A for p-type material is accomplished by substituting the valence-band density of states for N_c and using the expression[32]

$$f_i(\psi) = \{1+\beta_i^{-1}\exp[(E_i-\psi)/kT]\}^{-1} \tag{B1}$$

for the *ionization* probability of the ith *acceptor* level. Here energies E_i and ψ are interpreted to be measured with respect to the valence band edge. Now the expressions of Appendix A for $H(\psi)$ and $F(\psi,\omega)$ may be calculated numerically for any given ψ.

The integration of Eq. (10) is done numerically[33] from the initial value $W=0$ at $\psi=\mu_F$ to a final value at $\psi = V_B - V$. The initial slope, $dW/d\psi$, is

$$\left.\frac{dW}{d\psi}\right|_{\mu_F} = [F(\mu_F,0)/F(\mu_F,\omega)]^{1/2}. \tag{B2}$$

The resulting values of W are then used in Eq. (9) to determine the diode admittance. For the diode of Figs. 4 and 5, the admittance was calculated as a function of

temperature. The level densities, N_1, N_2, and N_3 were varied to obtain a good fit to the capacitance values in the plateau regions between the capacitance steps of Fig. 5. In this case the adjustment of the level densities was subject to the condition $N_1 + N_2 + N_3 = 4.8 \times 10^{18}$ (Sec. IV B).

[1]D. L. Losee, Appl. Phys. Lett. **21**, 54 (1972); this is a preliminary report of the present work.
[2]C. T. Sah, W. W. Chan, H. S. Fu, and J. W. Walker, Appl. Phys. Lett. **20**, 193 (1972).
[3]M. G. Buehler, Solid-State Electron. **15**, 69 (1972).
[4]D. V. Lang J. Appl. Phys. **45**, 3014 (1974).
[5]For example, R. Williams, J. Appl. Phys. **37**, 3411 (1966).
[6]For a review, see C. T. Sah, L. Forbes, L. L. Rosier, and A. F. Tasch, Jr., Solid-State Electron. **13**, 759 (1970).
[7]W. Shockley and W. T. Read, Jr., Phys. Rev. **87**, 835 (1952); R. N. Hall, Phys. Rev. **83**, 228 (1951).
[8]G. I. Roberts and C. R. Crowell, J. Appl. Phys. **41**, 1767 (1970).
[9]C. T. Sah and J. W. Walker, Appl. Phys. Lett. **22**, 384 (1973).
[10]Y. Zohta, Appl. Phys. Lett. **17**, 284 (1970); Solid-State Electron. **16**, 1029 (1973).
[11]J. A. Copeland, IEEE Trans. Electron Devices **ED-16**, 445 (1966).
[12]C. A. Mead and W. G. Spitzer, Phys. Rev. **134**, A713 (1964); R. H. Fowler, Phys. Rev. **38**, 45 (1931).
[13]M. Beguwala and C. R. Crowell, Solid-State Electron. **17**, 203 (1974).
[14]J. Maserjian, J. Vac. Sci. Technol. **6**, 843 (1969).
[15]G. H. Glover, IEEE Trans. Electron Devices **ED-19**, 138 (1972).
[16]M. Schulz, Appl. Phys. Lett. **23**, 31 (1973).
[17]J. R. Fischer, R. P. Khosla, Y. T. Tan, and D. K. Ranadive, J. Appl. Phys. **44**, 1708 (1973).
[18]M. R. Lorenz, B. Segall, and H. H. Woodbury, Phys. Rev. **134**, A751 (1964).
[19]G. W. Iseler, J. A. Kafalas, A. J. Strauss, H. F. MacMillan, and R. H. Bube, Solid State Commun. 10, 619 (1972); H. F. MacMillan, thesis (Stanford University, 1972) (unpublished).
[20]D. L. Losee, R. P. Khosla, D. K. Ranadive, and F. T. J. Smith, Solid State Commun. **13**, 819 (1973).
[21]E. Schibli and E. G. Milnes, Solid-State Electron. **11**, 323 (1968).
[22]For example, A. Rose, *Concepts in Photoconductivity and Allied Problems* (Interscience, New York, 1963).
[23]D. L. Losee and D. K. Ranadive, Bull. Am. Phys. Soc. **19**, 299 (1974); J. R. Fischer, R. P. Khosla, and B. C. Burkey, Bull. Am. Phys. Soc. **19**, 299 (1974).
[24]S. Teitler and R. F. Wallis, J. Phys. Chem. Solids **16**, 71 (1960).
[25]T. L. Larsen, C. F. Varotto, and D. A. Stevenson, J. Appl. Phys. **43**, 172 (1972).
[26]W. D. Baker and A. G. Milnes, J. Appl. Phys. **45**, 5152 (1972).
[27]H. Mannex, thesis (Air Force Institute of Technology, 1968) (unpublished).
[28]B. C. Burkey, R. P. Khosla, J. R. Fischer, and D. L. Losee (unpublished).
[29]We assume that there is a uniform positive background of ionized shallow donors, which is just compensated (see Refs. 19 and 28) by the double acceptors. Statistically, this is equivalent to treating the double-acceptor centers as donors in the calculation.
[30]J. S. Blakemore, *Semiconductor Statistics* (Pergamon, London, 1962).
[31]R. A. Stradling, Solid State Commun. **6**, 665 (1968).
[32]S. M. Sze *Physics of Semiconductor Devices* (Wiley, New York, 1969).
[33]For examples of such integration subroutines see IBM System/360 Scientific Subroutine Package (360A-CM-03X) Programmers Manual.